Journal of Applied Sciences

ISSN 1812-5654

science alert

ANSInet
an open access publisher
http://ansinet.com

Journal of Applied Sciences 8 (3): 394-406, 2008
ISSN 1812-5654

Nonlinear Analysis of RC Flanged Shear Walls Considering Tension-Stiffening Effect

Alireza Mortezaei and Ali Kheyroddin
Department of Civil Engineering, Faculty of Engineering, Semnan University, Semnan, Iran

Abstract: In order to analysis of reinforced concrete structures subjected to general loading conditions, realistic constitutive models and analytical procedures are required to produce reasonably accurate simulations of behavior. In this study, an analytical model which can predict the nonlinear behavior of Reinforced Concrete (RC) structures such as flanged shear walls subjected to shear and normal stresses is introduced. The proposed model includes the description of biaxial failure criteria which show compressive strength enhancement and tensile resistance reduction effects for the stress states of biaxial compression and tension-compression, respectively. After tensile cracking, concrete compressive strength degradation was implemented and the tensile capacity of concrete maintained by the reinforcing steel (tension-stiffening effect) is considered. Using the concept of average stresses and strains, a criterion is proposed to simulate the tension-stiffening effect based on the force equilibriums and compatibility conditions. The finite element model predictions are validated by comparison with available experimental data. In addition, correlation studies between analytical results and experimental values from idealized shear walls tests were conducted. Load-displacement relations of shear walls under various stress conditions are then evaluated to verify the accuracy of the proposed model.

Key words: Tension-stiffening effect, nonlinear analysis, flanged shear walls, finite element method

INTRODUCTION

As the need for the seismic design of civil structures increases, many experimental and analytical studies predicting the nonlinear response of structures according to the load increase and computing the ultimate resistance under extreme load conditions have been performed (ASCE, 1982). Due to the advantage of its rigidity, shear walls which offer great resistance for lateral loads have been widely adopted in building structures. Nevertheless, the design method mentioned in design codes does not always give a reasonable calculation since the shear wall capacity, as predicted on the basis of the truss analogy concept, often overestimates the structural behavior established by experiment. Therefore, nonlinear finite element analysis is definitely required to more exactly evaluate ultimate resisting capacity and load-deformation behavior.

In designing reinforced concrete frame-wall buildings, designers may choose nonplanar wall section, such as L, T, C etc., as opposed to planar shapes, such as rectangular or barbell. Responses of nonplanar walls with at least one cross-sectional principal axis that is not a symmetry axis are typically governed by unsymmetrical bending and would be influenced by inelastic biaxial interaction more significantly than those of planar walls. A related problem arises in evaluating the seismic vulnerability of frame-wall construction possessing significant plan irregularity (Palermo and Vecchio, 2004). It is necessary for an enhanced evaluation of structural behavior to model each constituent material and interaction between reinforcing steel and concrete appropriately. For the reinforced concrete finite element analysis of plane stress dominated structures such as shear walls, these phenomena should be considered in the analytical model: the strength criterion of concrete subjected to various combinations of biaxial stresses, variation in material properties before and after cracking, concrete cracking and crack propagation and the tension-stiffening behavior of reinforced concrete composite material.

Many mathematical models for the mechanical behavior of concrete are in use in the numerical analysis of Reinforced Concrete (RC) structures (ASCE, 1982). Among concrete constitutive relations, the orthotropic model that was developed based on the concept of equivalent uniaxial strain strikes a balance between accuracy and economy. Hence, it is being widely used for numerical analysis of reinforced concrete structures by many researchers (ASCE, 1982; Chen, 1982; Zienkiewicz *et al*., 2005).

Research significance: In this study, the first objective is to describe an analysis tool which is based on layered

Corresponding Author: Alireza Mortezaei, 192, Asjodi St., Baghferdos St., Semnan, Postal Code 35146-16953, Iran
Tel: 0098-9123313442 Fax: 0098-231-3332816

nonlinear finite element method (NONLACS2) and investigate nonlinear behavior of flanged shear walls. The second objective is presentation of analytical model with compressive strength degradation developed with Kwak RC panels (Kwak and Kim, 2006) and Vecchio's experimental study (Vecchio, 1999) in addition to the use of a model and a description of the strain softening region of concrete and tension-stiffening effect. The developed finite-element model is validated by comparison with test results from several idealized orthogonally reinforced concrete shear walls tested by Vecchio and Palermo (2002). In addition, to assess the applicability of the material model under different stress conditions, load-displacement relations and crack patterns are compared with flanged shear wall test results.

Nonlinear finite element program: A nonlinear finite element analysis program, NONLACS2 (NONLinear Analysis of Concrete and Steel Structures), developed by Kheyroddin (1996), is used to analyze the selected R.C. shear walls. The program employs a layered finite element approach and can be used to predict the nonlinear behavior of any plain, reinforced or prestressed concrete, steel, or composite concrete-steel structure that is composed of thin plate members with plane stress conditions. This includes beams, slabs (plates), shells, folded plates, box girders, shear walls, or any combination of these structural elements. Time-dependent effects such as creep and shrinkage can also be considered.

Concrete properties: The concrete behaves differently under different types and combinations of stress conditions due to the progressive microcracking at the interface between the mortar and the aggregates (transition zone). The propagation of these cracks under the applied loads contributes to the nonlinear behavior of the concrete. As shown in Fig. 1a, the uniaxial stress-strain curve of concrete adopted in this study, is made of two parts. The ascending branch up to the peak compressive strength is represented by the equation proposed by Ashour and Morley (1993):

$$\sigma = \frac{E_0 \varepsilon}{1 + \left(\frac{E_0}{E_{sc}} - 2\right)\left(\frac{\varepsilon}{\varepsilon_{max}}\right) + \left(\frac{\varepsilon}{\varepsilon_{max}}\right)^2} \quad (1)$$

Where:

E_0 = Initial modulus of elasticity of the concrete
E_{sc} = Secant modulus of the concrete at the peak stress
σ = Stress
ε = Strain
ε_{max} = Strain at peak stress

The descending or the strain-softening branch is idealized by the Bazant model (Bazant *et al*., 1986):

$$\sigma = \sigma_c \left(\frac{\varepsilon}{\varepsilon_{max}}\right) \exp\left(1 - \varepsilon/\varepsilon_{max}\right) \quad (2)$$

Where, σ_c is compressive strength of the concrete. For uniaxially loaded concrete, σ_c is equal to f'_c.

For analysis of most plane stress problems, concrete is assumed to behave as a stress-induced orthotropic material. In this study the orthotropic constitutive relationship developed by Darwin and Pecknold (1977) is used for modeling the concrete using the smeared cracking idealization. The constitutive matrix, D, is given by:

$$D = \frac{1}{(1-\nu^2)}\begin{bmatrix} E_1 & \nu\sqrt{E_1E_2} & 0 \\ \nu\sqrt{E_1E_2} & E_2 & 0 \\ 0 & 0 & \frac{1}{4}(E_1+E_2-2\nu\sqrt{E_1E_2}) \end{bmatrix} \quad (3)$$

in which, E_1 and E_2 are the tangent moduli in the directions of the material orthotropy and ν is the Poisson's ratio. The orthotropic material directions coincide with the principal stress directions for the uncracked concrete and these directions are parallel and normal to the cracks for the cracked concrete. The concept of the "equivalent uniaxial strain" developed by Darwin and Pecknold (1977) is utilized to relate the increments of stress and strain in the principal directions. Therefore, stress-strain curves similar to the uniaxial stress-strain curves can be used to formulate the required stress-strain curves in each principal direction.

The strength of concrete, σ_c and the values of E_1, E_2 and ν are functions of the level of stress and the stress combinations. The concrete strength when subjected to biaxial stresses is determined using the failure envelope developed by Kupfer *et al*. (1969). The values of E_1 and E_2 for a given stress ratio ($\alpha = \sigma_1/\sigma_2$) are found as the slopes of the σ_1-ε_1 and σ_2-ε_2 curves, respectively. For the descending branches of both compression and tension stress-strain curves, E_i is set equal to a very small number, 0.0001, to avoid computational problems associated with a negative and zero values for E_i. The concrete is considered to be crushed, when the equivalent compressive strain in the principal directions exceeds the ultimate compressive strain of the concrete, ε_{cu}. For determination of the concrete ultimate compressive strain, ε_{cu}, two models for unconfined high and normal-strength concrete (Pastor, 1986) and confined concrete (Chung *et al*., 2002) are implemented into the program.

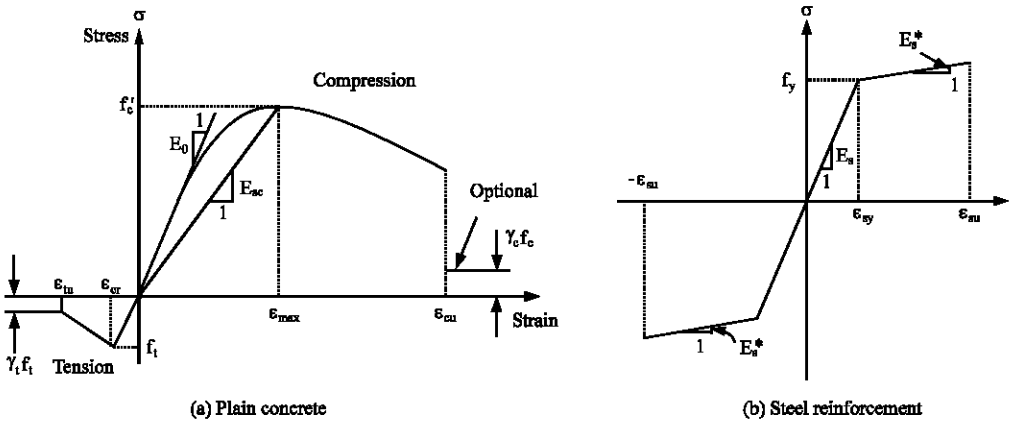

Fig. 1: Uniaxial stress-strain curves

For elimination of the numerical difficulties after crushing ($\varepsilon>\varepsilon_{cu}$) and cracking of the concrete ($\varepsilon>\varepsilon_{tu}$), a small amount of compressive and tensile stress as a fraction of concrete strength, $\gamma_c f'_c$ and $\gamma_t f'_t$, is assigned (optional) at a high level of stress (Fig. 1a), where parameters γ_c and γ_t define the remaining compressive and tensile strength factors, respectively.

Crack modeling techniques: Cracking of the concrete is one of the important aspects of material nonlinear behavior of the concrete. Besides reducing the stiffness of the structure, cracks have resulted in redistribution of stresses to the reinforcing steel as well as increasing the bond stress at the steel-concrete interface (Sundara *et al.*, 2002). Cracking of the concrete is idealized using the fixed smeared cracking model and is assumed to occur when the principal tensile stress at a point (usually a Gauss integration point) exceeds the tensile strength of the concrete. After cracking, the axes of orthotropy are aligned parallel and orthogonal to the crack. The elastic modulus perpendicular to the crack direction is reduced to a very small value close to zero and the Poisson effect is ignored. The effect of the crack is smeared within the element by modifying the [D] matrix. If σ_1 exceeds the tensile strength of concrete, f'_t, the material stiffness matrix is defined as (one crack is opened):

$$[D]=\begin{bmatrix}0 & 0 & 0\\ 0 & E_2 & 0\\ 0 & 0 & \beta G\end{bmatrix} \quad (4)$$

Where, $0<\beta\leq 1.0$

Once one crack is formed, the principal directions are not allowed to rotate and a second crack can form only when $\sigma_2>f'_t$, in a direction perpendicular to the first crack. Then,

$$[D]=\begin{bmatrix}0 & 0 & 0\\ 0 & 0 & 0\\ 0 & 0 & \beta G\end{bmatrix} \quad (5)$$

Where, $0<\beta\leq 1.0$

The shear retention factor, β, with a value of less than unity, serves to eliminate the numerical difficulties that arise if the shear modulus is reduced to zero and more importantly, it accounts for the fact that cracked concrete can still transfer shear forces through aggregate interlock and dowel action. Due to the bond between the concrete and the steel reinforcement, a redistribution of the tensile stress from the concrete to the reinforcement will occur (Martín-Pérez and Pantazopoulou, 2001). In fact, the concrete is able to resist tension between the cracks in the direction normal to the crack; this phenomenon is termed tension-stiffening. The tension-stiffening effect is idealized by assuming the ascending and the descending branches of the tensile stress-strain curve that is described in the next section. For evaluation of an appropriate value of the ultimate tensile strain of the concrete, ε_{tu} and elimination of mesh size dependency phenomenon, Kheyroddin *et al.* (1997) proposed the following simple formula:

$$\varepsilon_{tu} = 0.004\ e^{-0.008\ h} \qquad (\varepsilon_{tu} \geq \varepsilon_{cr}) \quad (6)$$

Where:

h = Width of the element in mm

ε_{cr} = Concrete cracking strain

For elimination of the element size effect phenomenon, both the new proposed model and the crack band model, based on fracture mechanics, proposed by Bazant and Oh (1983) have been implemented into the NONLACS2 program.

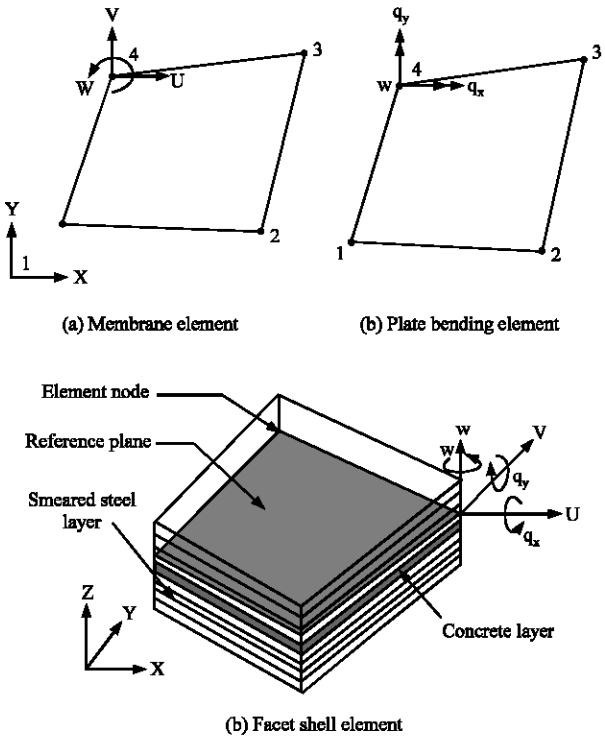

Fig. 2: Some typical finite elements in NONLACS2 Program

Reinforcing bar properties: The reinforcing bars are modeled as an elastic strain-hardening material as shown in Fig. 1b. The reinforcing bars can be modeled either as smeared layers or as individual bars. In both cases, perfect bond is assumed between the steel and the concrete.

Finite element formulation: The element library includes plane membrane, plate bending, one dimensional bar, shear connecter, spring boundary elements as well as a facet shell element, which is a combination of the plane membrane and the plate bending elements. Figure 2 shows some of these elements and the associated degrees of freedom. The two nodes, three degrees of freedom per node one dimensional bar element is used to model uniaxial truss members, unbonded prestressed tendons and shear connectors. The program employs a layered finite element approach. The structure is idealized as an assemblage of thin constant thickness plate elements with each element subdivided into a number of imaginary layers as shown in Fig. 2c. A layer can be either of concrete, smeared reinforcing steel or a continuous steel plate. The number of layers depends on the behavior of the structure being analyzed. Each layer is assumed to be in a state of plane stress and can assume any state-uncracked, partially cracked, fully cracked, non-yielded, yielded and crushed-depending on the stress or strain conditions.

Nonlinear analysis method: Nonlinear analysis is performed using an incremental-iterative tangent stiffness approach and the element stiffness is obtained by adding the stiffness contributions of all layers at each Gauss quadrature point. The change in the material stiffness matrix during loading necessitates an incremental solution procedure with a tangent stiffness scheme that using piece-wise linearization has been adopted in the NONLACS2 program.

Tension-stiffening model: Cracking in concrete will develop and propagate in the direction normal to that of the major principal strain starting from the section where a crack first originates. Even after cracking, however, concrete is still partially capable of resisting tensile forces due to the bond between concrete and reinforcement. This phenomenon which results from crack formation and the bond between steel and its surrounding concrete is defined as the tension stiffening effect. This effect can be adequately accounted for by increasing the average stiffness of the element which has relatively large dimensions when compared with the size of the cracked section. An increase in the tensile stiffness of concrete can be accomplished by using a stress-strain relation which includes a descending branch in the tension region.

Many experimental studies to predict the post-cracking behavior of reinforced concrete structures have been conducted and several analytical models using the fracture energy concept or bond mechanisms have been developed (Gupta and Maestrini, 1989; Hegemier *et al*., 1985). In this study, based on the force equilibriums, compatibility conditions and the bond-stress-slip relationship between reinforcement and the surrounding concrete in the principal tensile direction, a descending branch to define the post-cracking stress-strain relation of concrete is proposed. Differently from most of the analytical models which consider the tension stiffening effect in a uniaxial stress state along the reinforcing steel (Gupta and Maestrini, 1990; Choi and Cheung, 1996), the effect according to the reinforcing steel in both directions are directly included in the softening branch of concrete and the cracking which is not normal to the reinforcing steel can be simulated effectively.

Force equilibriums: A cracked reinforced concrete element subjected to membrane stresses is shown in

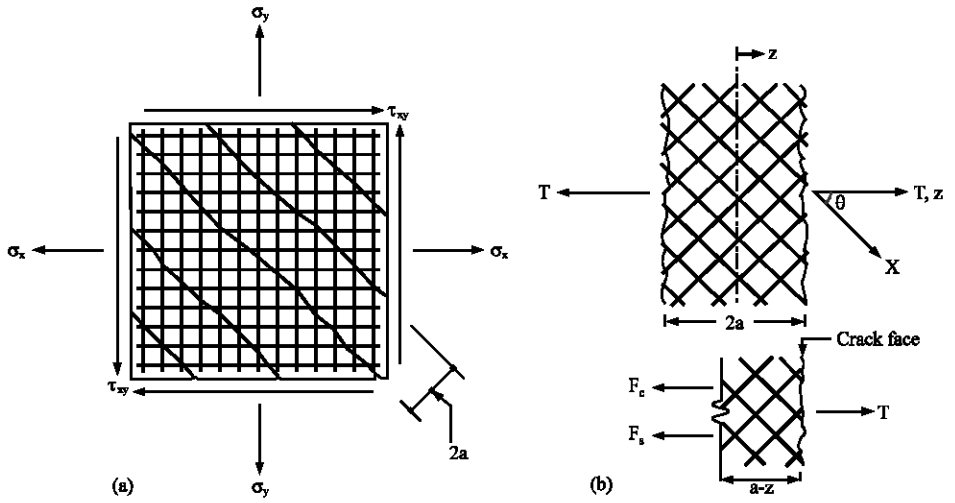

Fig. 3: Descriptions for (a) cracked RC planar element and (b) force equilibrium in the arbitrary section

Fig. 3a and a part of the element along the inclined crack faces with crack spacing of 2a can be taken as the free body diagram Fig. 3b. If the z direction is normal to the crack surface, it makes an angle θ with the x direction and coincides with the principal tensile strain axis.

Since the applied principal tensile force of RC membrane element, T, is carried partly by the concrete matrix (F_c) and partly by the reinforcing steel (F_s), the following force equilibrium equation is obtained:

$$T = F_c + F_s \tag{7}$$

Using the equivalent steel modulus of elasticity, $E_{s,eq}$ calculated from the force equilibrium with respect to the principal tensile direction and expressed in terms of the reinforcement ratio and elastic modulus of steel in each direction, the force component carried by steel can be rearranged as:

$$\begin{aligned} F_s &= E_{S,eq}\varepsilon_{s1}A_{c1} \\ E_{s,eq} &= E_{sx}\rho_x\cos^4\theta + E_{sy}\rho_y\sin^4\theta \end{aligned} \tag{8}$$

Where:

ε_{s1} = Steel strain about the z direction

A_{c1} = Cross-section area of concrete perpendicular to the z direction and as before, θ is the angle between the direction normal to the crack and the global x direction.

Also, the force component carried by concrete can be expressed by:

$$F_c = E_c\varepsilon_{1u}A_{c1} = E_c\frac{1}{1-\nu^2}\left(\varepsilon_1 + \nu\sqrt{\frac{E_2}{E_c}}\varepsilon_2\right)A_{c1} \tag{9}$$

Where, ε_{1u} means the equivalent uniaxial strain along the z direction. E_2, representing the elastic modulus of concrete in the orthogonal direction to the z direction, varies according to the loading history, while E_1 in the principal tension direction (z direction) is the same as the initial elastic modulus of concrete E_c and does not change with increasing principal tensile strain because the concrete between cracks still remains as an uncracked elastic material.

Reinforcing bars transfer tensile stresses to the concrete through the bond stresses along the surface between reinforcements and surrounding concrete, so that an infinitesimal element of length dz is taken out from the intact concrete between cracks to obtain the equilibrium equations for the concrete and steel. Figure 4 represents the free body diagrams at the steel and concrete interfaces.

Based on the force equilibrium at the steel interface, the steel force variation can be derived in terms of the bond stresses:

$$dF_s = \left(p_x n_x f_{bx}\frac{dz}{\cos\theta}\right)\cos\theta + \left(p_y n_y f_{by}\frac{dz}{\sin\theta}\right)\sin\theta \tag{10}$$

in which p is the perimeter of a reinforcing bar, n is the number of bars placed within an infinitesimal length dz, f_b is the bond stress at the steel-concrete interface and the subscripts x and y denote the x and y directions, respectively.

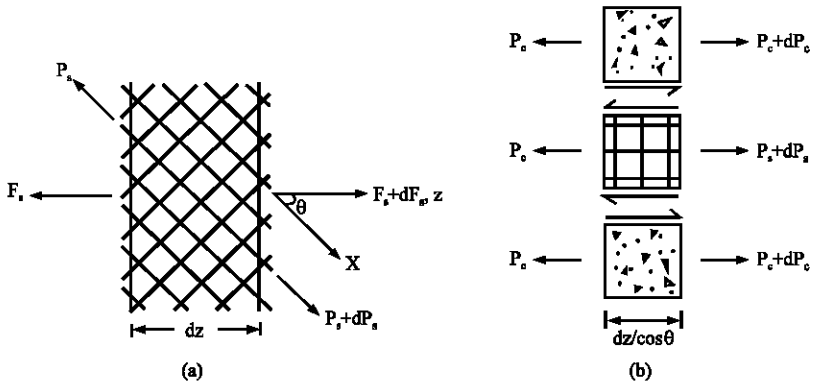

Fig. 4: Free body diagrams for (a) the RC element and (b) steel and concrete interfaces

Assuming that the bond stresses are identical in the x and y directions, the following equilibrium equations for the steel and concrete can be obtained:

$$\frac{dF_s}{dz} = pnf_b, \qquad \frac{dF_c}{dz} = -pnf_b \tag{11}$$

Where:

$pnf_b = p_x n_x + p_y n_y) f_b$

Bond slip behavior: Since the bond-slip (Δ) at the steel-concrete interface is defined by the relative displacement between the reinforcing steel and concrete ($\Delta = u_s - u_c$), substitution of (8) and (9) into the second order differential equation of bond-slip leads to:

$$\begin{aligned}\frac{d^2\Delta}{dz^2} &= \frac{d^2u_s}{dz^2} - \frac{d^2u_c}{dz^2} \\ &= \frac{d}{dz}\left(\frac{F_s}{E_{s,eq}A_{cl}}\right) - \frac{d}{dz}\left((1-\nu^2)\varepsilon_{1u} - \nu\sqrt{\frac{E_2}{E_c}}\varepsilon_2\right) \\ &= \frac{1}{E_{s,eq}A_{cl}}\frac{dF_s}{dz} - \frac{1-\nu^2}{E_cA_{cl}}\frac{dF_c}{dz},\end{aligned} \tag{12}$$

Where:

$d\varepsilon_2/dz = 0$

After substituting Eq. 11 into 12 and then if the linear bond stress-slip relationship of $f_b = E_b\Delta$ is assumed, the governing differential equation is obtained:

$$\frac{d^2\Delta}{dz^2} - k^2\Delta = 0 \tag{13}$$

Where:

$k^2 = (pnE_b/A_{cl})\,(1/E_{s,eq} + 1\text{-}\nu^2/E_c)$

E_b = Slip modulus

The general solution to Eq. 13 is given by $\Delta = C_1\sinh kz + C_2\cosh kz$, in which C_1 and C_2 are constants that have to be determined from the boundary conditions. Because of symmetry, the slip should be zero at the center ($z = 0$) of the segment and $\Delta(-z) = -\Delta(z)$ must be satisfied Fig. 3b. Hence, $C_2=0$ is determined. Integration of Eq. 11 after substituting the obtained general solution leads to the following expression for the steel force F_s:

$$F_s = \frac{pnE_bC_1}{k}\cosh kz + C_3 \tag{14}$$

Where, the constant of integration $C_3 = T - (pnE_bC_1/k)\times\cosh(ka)$ is obtained from the boundary condition at the crack surface ($F_s = T$ at $z = a$). Moreover, the displacement of reinforcement is obtained from Eq. 8.

$$u_s = \frac{Tz}{E_{s,eq}A_{cl}} - \frac{C_1}{\left(1 + E_{s,eq}\dfrac{1-\nu^2}{E_c}\right)}(kz\cosh ka - \sinh kz) \tag{15}$$

Through the same procedure, the resisting force and displacement y the concrete matrix are also determined as:

$$F_c = \frac{pnE_bC_1}{k}(\cosh ka - \cosh kz) \tag{16}$$

$$u_c = \frac{E_{s,eq}\dfrac{1-\nu^2}{E_c}C_1}{1 + E_{s,eq}\dfrac{1-\nu^2}{E_c}}(kz\cosh ka - \sinh kz) \tag{17}$$

in which $C_1=(T/E_{s,eq}A_{cl})(1/k\cosh ka)$ is determined from (15) and (17).

Tension-stiffening model: ased on the obtained equations, a descending branch in the tension region of the concrete stress-strain relation can be determined. First, the equilibrium Eq. 7 is:

$$T = E_{s,eq}\varepsilon_{s1}A_{c1} + \sigma_c A_{c1} \tag{18}$$

Where, the term σ_c s the effective tensile stress in concrete and ε_{s1} is the average strain in the reinforcing bar. These values can be obtained from (15) and (18).

$$\varepsilon_{sl} = \frac{u_s(z=a)}{a} = \frac{T}{E_{s,eq}A_{cl}}\left(1 - \frac{\left(1 - \frac{\tanh ka}{ka}\right)}{1 + E_{s,eq}\frac{1-\nu^2}{E_c}}\right) \tag{19}$$

$$\sigma_c = \frac{1}{A_{cl}}\left(\frac{T\left(1 - \frac{\tanh ka}{ka}\right)}{1 + E_{s,eq}\frac{1-\nu^2}{E_c}}\right) \tag{20}$$

The maximum tensile force in concrete occurs at x = 0. Hence, from Eq. 16, this maximum force can be obtained as:

$$F_{c,max} = \frac{T(1 - \operatorname{sech} ka}{1 + E_{s,eq}\frac{1-\nu^2}{E_c}} \tag{21}$$

The corresponding concrete stress is $\sigma_{c,max} = F_{c,max}/A_{c1}$, that is, the maximum tensile stress in concrete is directly proportional to the applied principal tensile force T. Accordingly, $\sigma_{c,max}$ converges to the tensile strength of concrete, f'_t as the applied tensile force T increases. At that point, a new crack will be formed at z = 0. After eliminating T from (19) and (20), those are rewritten in a nondimensional form:

$$\frac{\sigma_c}{f'_t} = \frac{1 - \frac{\tanh ka}{ka}}{1 - \operatorname{sech} ka} \tag{22}$$

$$\frac{\varepsilon}{\varepsilon_{crack}} = \frac{\left(1-\nu^2\right) + \frac{\tanh ka}{(n'_x\rho_x \cos^4\theta + n'_y\rho_y \sin^4\theta)ka}}{1 - \operatorname{sech} ka} \tag{23}$$

Where, $\varepsilon_{crack} = f'_t/E_c$, n'_x and n'_y are the modular ratios in the x and y directions, respectively.

In Eq. 22, σ_c/f'_t converges to the value of 2/3 as the parameter ka related to crack spacing approaches zero. However, the actual crack spacing is not narrowed any more but remains constant after reaching a certain value. The experimental study by Campione and Mendola (2004) indicates that the number of cracks is stabilized when the average strain is about 0.001. Therefore, with the assumption that the linear bond stress-slip relation remains, (22) and (23) can be available up to ε = 0.001.

Further deformation leads to the yielding of the reinforcing steel, followed by the increase of the slip while maintaining a plateau $f_b = \tau_b$. For more increase of the slip, the bond stress decreases linearly to the value of the ultimate frictional bond resistance (ASCE, 1982). In the case of constant bond stress ($f_b = \tau_b$) and the yielding of the reinforcing steel, the principal tensile force carried by each material can be calculated from Eq. 11 with appropriate boundary conditions Fig. 3b.

$$F_s = T - pn\tau_b(a - z), \qquad F_c = pn\tau_b(a - z) \tag{24}$$

From Eq. 8, the displacement of steel can be expressed by

$$u_s = \frac{1}{E_{s,eq}A_{cl}} z\left(T - pn\tau_b\left(a - \frac{z}{2}\right)\right) \tag{25}$$

Moreover, the average strain in the reinforcing steel, ε_{s1}, can be obtained by differentiating u_s with respect to z and substituting a for z, that is, $\varepsilon_{s1}=(1/E_{s,eq}A_{c1})(T^{-}pn\tau_b a/2)$. Accordingly, the effective tensile stress of concrete can be calculated from Eq. 18 with $\varepsilon_{s1}(\sigma_c = 1/A_{c1}\bullet pn\tau_b a/2)$. The nondimensional parametric equations for σ_c/f'_t and $\varepsilon/\varepsilon_{crack}$, as was done in the case of the linear bond stress-slip relationship, are determined as follows:

$$\frac{\sigma_c}{f'_t} = \frac{1}{2} \tag{26}$$

$$\frac{\varepsilon}{\varepsilon_{crack}} = \frac{1}{E_{s,eq}}\left(T - \frac{pn\tau_b a}{2}\right)\frac{E_c}{pn\tau_b a} \tag{27}$$

Where, $f'_t = pn\tau_b a/A_{c1}$ from Eq. 24. The principal tensile force T is given by $T = f_{yx}\rho_x A_x \cos\theta + f_{yy}\rho_y A_y \sin\theta$ in which f_y is the yield strength of steel, ρ is the reinforcement ratio, A is the cross-section area normal to the crack surface of concrete and the subscripts x and y mean the x and y directions, respectively. A similar result of σ_c/f'_t = 1/2 was introduced by Gupta and Maestrini (1990). Substituting the relation of T into Eq. 27 yields the following equation represented in terms of material parameters only:

$$\frac{\varepsilon}{\varepsilon_{crack}} = \frac{1}{E_{s,eq}}\left(t\left(f_{yx}\rho_x \cos\theta + f_{yy}\rho_y \sin\theta\right) - \frac{\frac{p}{s}\tau_b a}{2}\right)\frac{E_c}{\frac{p}{s}\tau_b a} \tag{28}$$

in which $p/s = (p_x/s_x)+(p_y/s_y)(l_y/l_x)$, t is the thickness of the RC element, s_x and s_y are the spacings of reinforcements and l_x and l_y are the length of sides normal to the x and y directions, respectively.

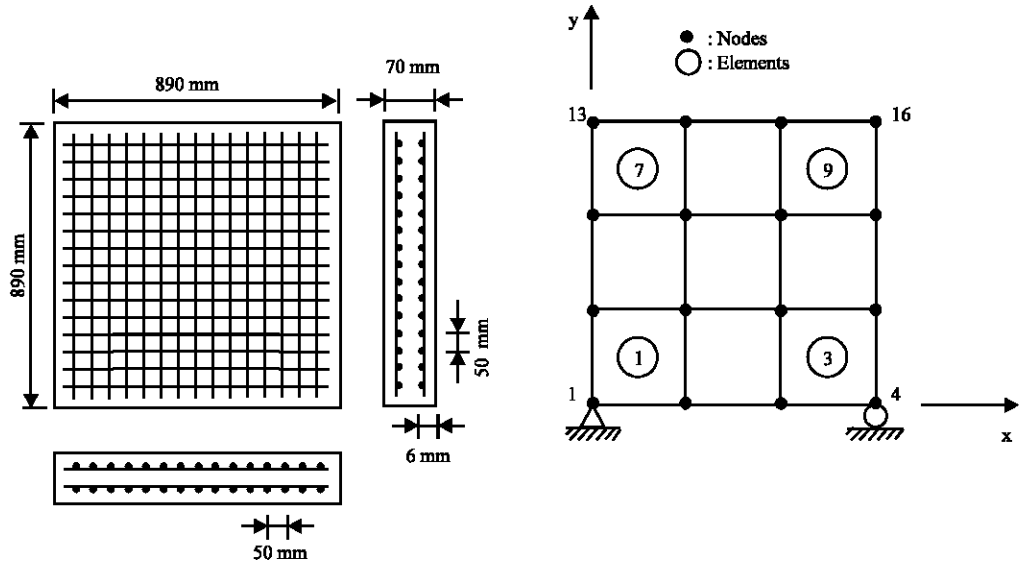

Fig. 5: Configuration and finite element idealization of panels

Finally, the boundary value of the strain corresponding to $\sigma_c = 0$ is calculated from the relation of $T = F_s + F_c$ with $F_c = 0$ through the same procedure.

$$\frac{\varepsilon}{\varepsilon_{crack}} = \frac{t\left(f_{yx}\rho_x \cos\theta + f_{yy}\rho_y \sin\theta\right)}{E_{s,eq}} \frac{E_c}{\frac{p}{s}\tau_b a} \quad (29)$$

τ_b is considered a material property and its magnitude depends on many factors. When τ_b is known from measurements, the descending branch of the tension region can be defined exactly. For computational convenience, τ_b = 5 MPa generally assumed in many numerical analyses was adopted in this study. Also, half an average crack spacing, a(S_{ave} = 2a), is determined by using $S_{max} = (\cos\theta/S_{x,max} + \sin\theta/S_{y,max})^{-1}$ and $S_{ave} = 0.75\ S_{max}$ introduced by Campione and Mendola (2004).

Applications: The capability of NONLACS2 program to reliably simulate the fundamental behavior arising from elastic and inelastic flexure interaction was verified by correlating analytically simulated and measured response of three works. In each case, different forms of output (including mode of failure) were extracted and compared with experimental results to verify key aspects of the numerical model. Although some discrepancies were observed, the overall match between the analytical models and experimental tests was good.

Kwak and Kim RC shear panels: The experimental results from reinforced concrete shear panels tested by Kwak and Kim (2006) are widely used to validate the analytical models for reinforced concrete membrane element. These panels were orthogonally reinforced and had identical dimensions of 890×890×70 mm. Lateral load was imposed on the top-right joint and the axial load was spread along the top rows of joint. Figure 5 shows the configuration of the test specimen and the finite element grid used. The finite element used in this study is an isoparametric four node element with 2×2 Gauss integration because all the stresses at every Gauss point are the same values and the four node element gives more stable stress results through the loading history. The assumed material properties were as follows: Poisson's ratio $\nu = 0.2$, the tensile strength of concrete, $f_c' = 0.33\sqrt{f_c'}$ MPa, the elastic modulus of steel E_{s1} = 200,000 MPa, $E_{s2} = 0.01\ E_{s1}$.

A two-dimensional static monotonic analysis was performed by Kwak and Kim (2006). For modeling of shear wall in NONLACS2 program, have been used four-node shell elements, QLC3 type as plane stress and bending. Results analyses are plotted in Fig. 6 along with the envelope response of the two-dimensional pushover analysis and the experimental response of the specimen. In spite of the exact predictions in the failure modes, the analysis slightly overestimates the shear strength of the panels. In addition, the numerical results still give more exact predictions for the shear strength of a shear dominant structure because the prediction by code guidelines represents the large overestimate. Totally, the result indicated that NONLACS2 programs provide reasonable results and can be used to approximate ultimate load. An ultimate load of 1390 KN was reported for shear panel.

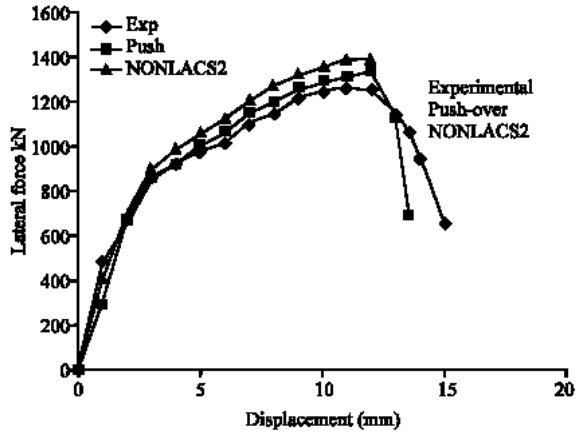

Fig. 6: Comparison of experimental and analytical results of Kwak and Kim RC shear panels

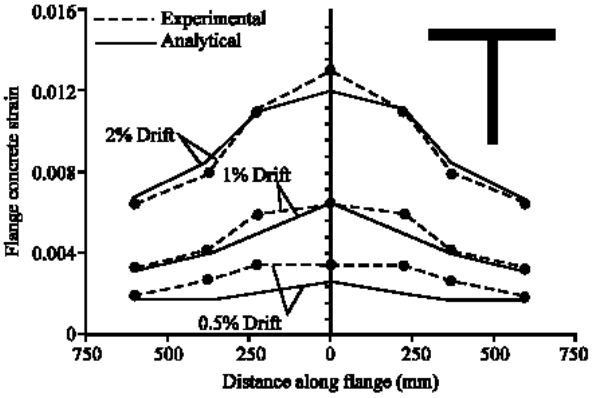

Fig. 7: Measured and computed tension flange strain profile for Specimen TW2

Wallace and Thomsen flanged walls (1995): Wallace and Thomsen (1995) conducted tests of T-shaped RC walls subjected to axial compression and cyclic lateral loading. Using measured material properties and dimensions, the monotonic and cyclic responses of Wall TW2 are calculated and compared with the test results. The measured and calculated load-deflection curves match well. As shown in Fig. 7, the measured strain distribution in the flange under tension also compares well to the computed strains for various drift levels. Because the model cannot capture local bar buckling, it was unable to predict the initiation of these modes of failure as observed in the tests. Nevertheless, the analytical results correlate well to the test data prior to the occurrence of these local modes of failure.

Vecchio and Palermo flanged walls (2002): The proposed material and tension-stiffening models were also applied to two large-scale flanged shear walls tested under static

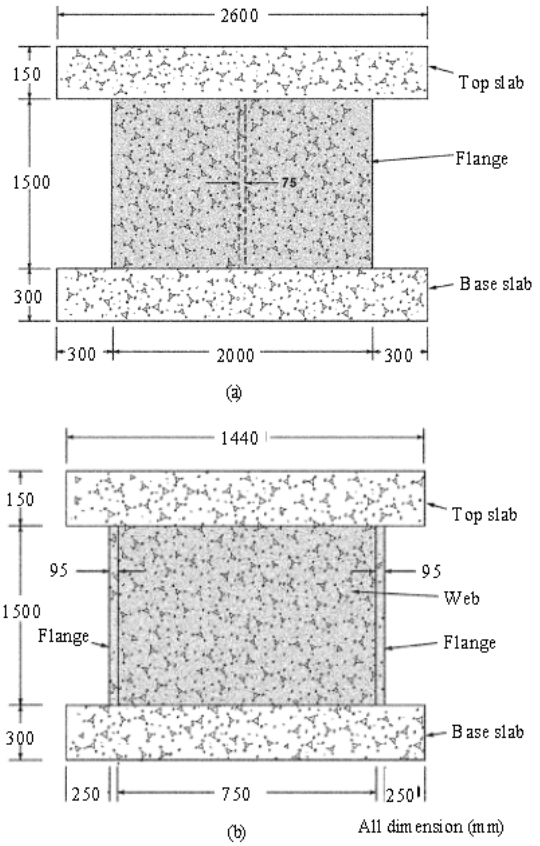

Fig. 8: Test specimen details: (a) end view and (b) side view

cyclic displacement by Vecchio and Palermo (2002). The specimens were constructed with stiff top and bottom slabs. The top slabs (2600×1440×150 mm) served to distribute the horizontal and axial load to the walls of the structure. The bottom slab (2600×1440×300 mm), clamped to the laboratory strong floor, simulated a rigid foundation. The slabs were reinforced with No. 30 (29.9 mm) deformed reinforcing bars at a spacing of 350 mm in each direction, with a top and bottom layer. Two types of walls, that is, Type I, 1000 mm wide ×1000 mm high × 70 mm thick (h/l = 1) and Type II, 750 mm wide × 1500 mm high × 65 mm thick (h/l = 2), were tested. The web wall was reinforced with D6 reinforcing bars, the bars were spaced 140 mm horizontally and 130 mm vertically in two parallel layers. The two flange walls were approximately 2000 mm long, 1000 and 1500 mm high and 95 mm thick. The flanges were also reinforced with D6 reinforcing bars, spaced 140 mm horizontally and 130 mm vertically near the web wall and 255 mm near the tips of the flanges. The concrete clear covers in the walls and slabs were 15 and 50 mm, respectively. Dimensional

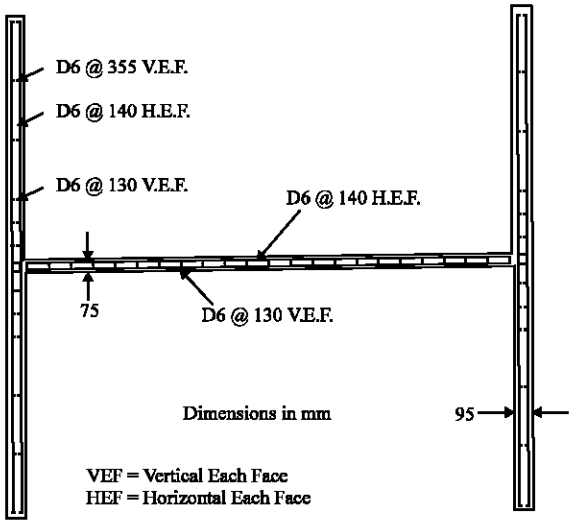

Fig. 9: Top view of wall reinforcement

details of the walls are shown in Fig. 8 and the reinforcement layout for the web and flange walls are given in Fig. 9 and 10.

The finite element mesh, shown in Fig. 11, consisted of 540 constant strain rectangular elements. The mesh was divided into four zones: the web wall, flange walls, top slabs and bottom slabs. For modeling of I-shaped shear wall in NONLACS2 program, have been used four-node shell elements, QLC3 type as plane stress and bending.

The shear wall specimens were subjected to the combined action of the uniformly distributed axial load and the horizontal load which was monotonically increased to failure. Type I shear walls SW13 and SW16 and Type II SW21, SW22, SW24 and SW25 were selected for the correlation study. Table 1 includes the material properties of concrete and the loading conditions. The material properties not mentioned in Table 1 are as follows: the uniaxial compressive strength of concrete, $f_c' = 0.85\ f_{cu}$, where f_{cu} is the cube strength. The tensile strength of concrete, $f_t' = 0.33(f_c')^{1/2}$ and the yield strength of vertical and horizontal reinforcements were 470 MPa and 520 MPa, respectively. All these values except f_t' are from the experimental data by Vecchio and Palermo (2002).

In order to investigate the contribution of the tension-stiffening effect to the structural response, the analytical results with and without tension-stiffening effect are compared with the measured load-displacement relations in Fig. 12. It is clear from the comparison of these results with the experimental data that the consideration of tension-stiffening effect yields a very satisfactory agreement for the structural stiffness and ultimate capacity as in the previous examples.

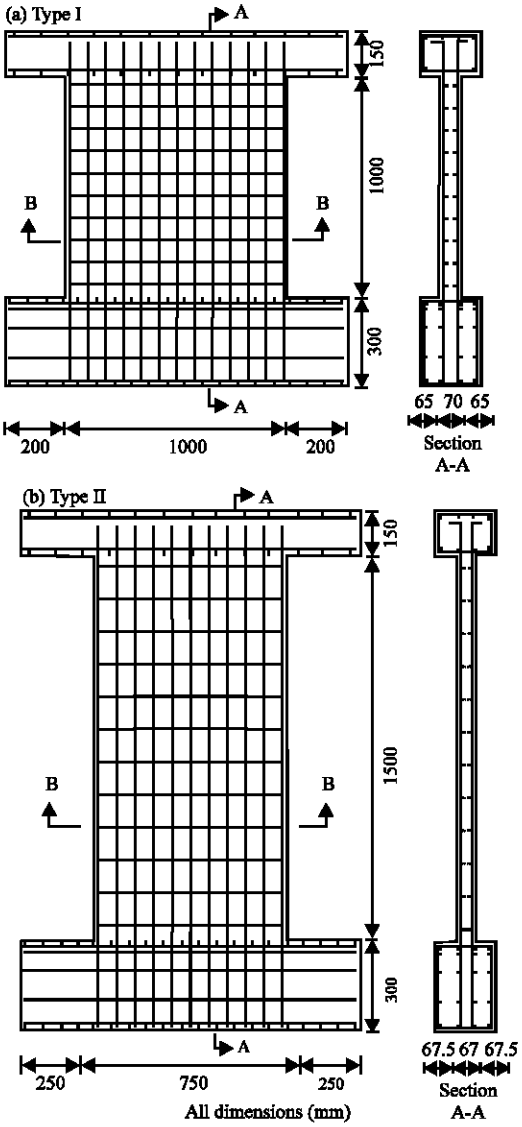

Fig. 10: Geometries and reinforcement details of Vecchio and Palermo flanged shear walls

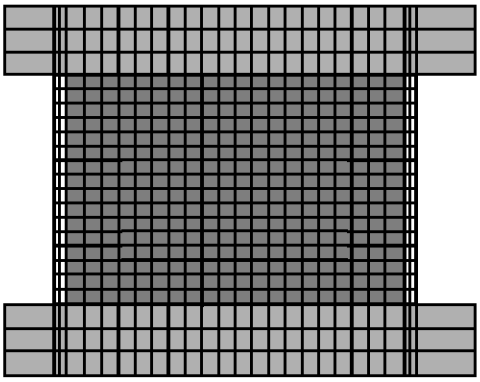

Fig. 11: Finite element mesh configuration

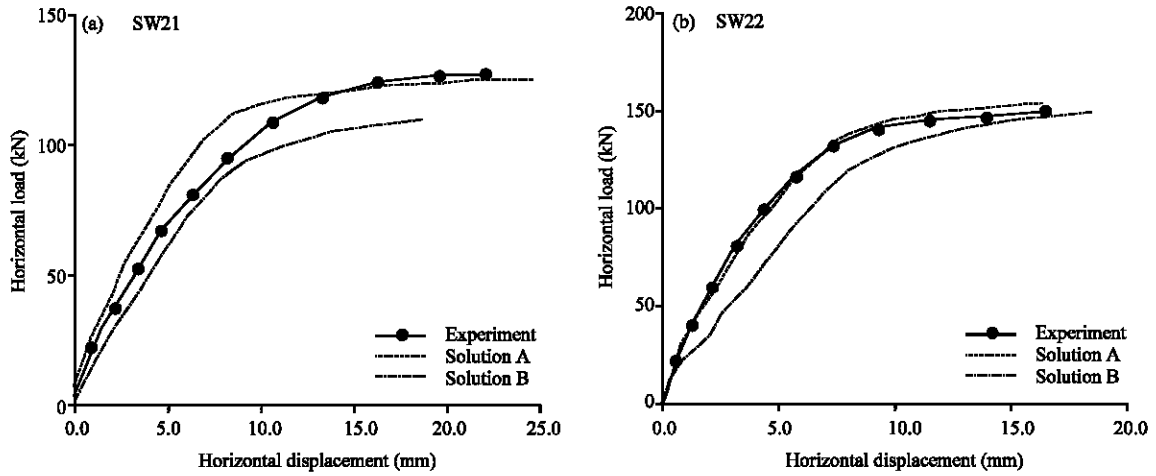

Fig. 12: Influence of tension-stiffening effect in shear walls SW21 and SW22. Solution (a) with tension-stiffening and solution (b) without tension-stiffening

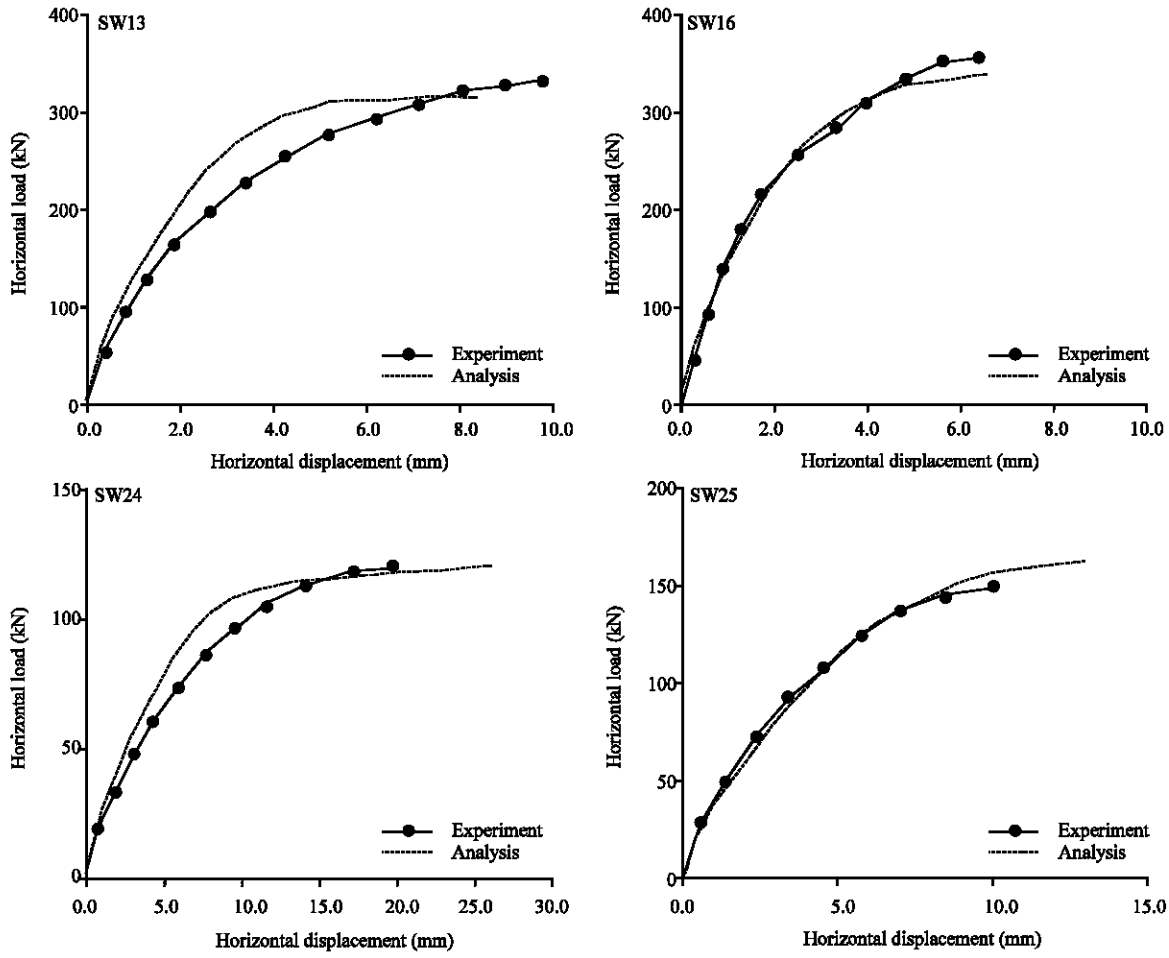

Fig. 13: Horizontal load versus top horizontal displacement for shear walls

Table 1: Loading conditions and material properties of shear walls

Wall	Specimen	Axial load (kN)	f'_c (MPa)	f'_t (MPa)	E_c (Mpa)
Type I	SW13	355	-34.5	1.94	29362
	SW16	460	-43.9	2.19	33132
Type II	SW21	0	-36.4	1.99	30207
	SW22	182	-43.0	2.16	32824
	SW24	0	-41.1	2.12	32109
	SW25	325	-38.3	2.04	30887

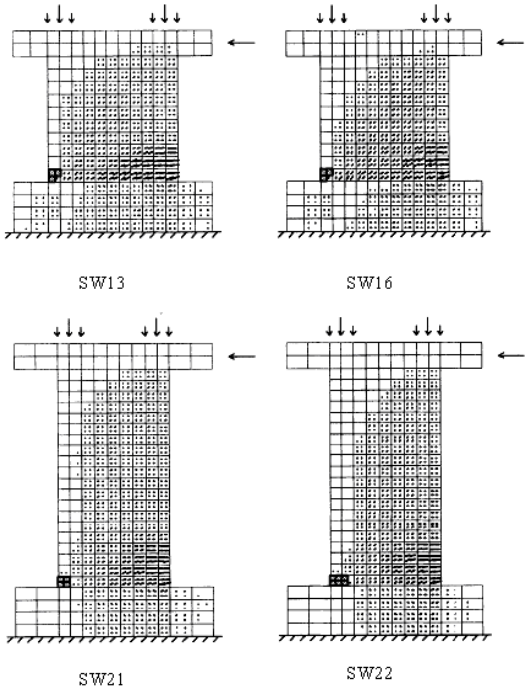

Fig. 14: Cracking and crushing patterns of shear walls at ultimate load level

As shown in Fig. 13, the lateral stiffness of RC structures is significantly affected by the level of axial force. This is basically caused by the fact that the applied compressive stress reduces the tensile stress as in the prestressed concrete structure, the confinement effect. Figure 14 shows the tensile cracking and compressive crushing pattern of specimens SW13, SW16, SW21 and SW22 at ultimate load. This figure verifies the propagated tensile cracks and compressive crushing failure reported by Vecchio and Palermo (2002). Similar tensile cracking and crushing patterns have been observed by Vecchio (1999) in his analytical runs for the same specimens.

The enhanced prediction can be obtained by considering the material nonlinearity and interaction parameters such as the fixed smeared cracking model, tension stiffening effect and bond-slip characteristics in the analysis of RC shear walls and panels (Kwak and Kim, 2004; van der Put, 2007).

CONCLUSIONS

An analytical model is proposed for the nonlinear finite element analysis of RC structures. Based on the concept of equivalent uniaxial strain, a concrete material model is presented in the axes of orthotropy which coincides with the principal axes of total strain and rotation during the load history. The applicability of the proposed orthotropic constitutive model in finite element analysis is verified by comparison with the reliable experimental results of the concrete stress-strain relations and load-displacement relations. Moreover, the tension-stiffening model introduced in this study may give the theoretical background for Vecchio's experimentally developed model which has been broadly adopted in many numerical analyses of RC structures.

The correlation studies between analytical results and test values and the parametric studies associated with them lead to the following conclusions: (1) the inclusion of tension-stiffening is important even in the structure dominantly affected by shear, (2) in the shear wall which is anisotropically reinforced and whose post-cracking behavior is dominated by the yielding of steel, the crack angle changes according to the loading history. Hence, fixed smeared cracking model must be adopted to exactly predict the cracked structural behavior, (3) for heavily reinforced shear walls, the global response of the panels is not dominantly affected by the tension-stiffening parameter but governed by concrete crushing. Therefore, compression softening due to tensile cracking should be considered and (4) the analyses of shear walls under a horizontal load verify strength enhancement as the uniformly distributed axial load increases.

ACKNOWLEDGMENTS

The research reported in this study was made possible by the financial supports from the Semnan University by the Ministry of Science and Technology of Islamic Republic of Iran. The authors would like to express their gratitude to organization for their support.

NOTATIONS

$[D]$ = Constitutive matrix
E_1,E2 = The tangent moduli in the directions of the material orthotropy
E_i = Tangent moduli in principal directions i; i = 1, 2
E_0 = The initial modulus of elasticity of the concrete
E_{sc} = The secant modulus of the concrete at the peak stress
E_s = Modulus of elasticity of reinforcement
f'_c = Compressive strength of concrete

f'_t = Direct tensile strength of concrete
f_y, f_{sy} = Yield strength of reinforcement bar
f_{su} = Ultimate stress of reinforcement
h = Width of the element
h_w = Wall height
α = Loading type factor
β = Shear retention factor
γ_c = The remaining compressive strength factor
γ_t = The remaining tensile strength factor
ε = Strain
ε_c = The strain of concrete
ε_{max}, ε_0 = The maximum compressive strain of the concrete
ε_{cu} = The ultimate compressive strain of the concrete
ε_{cr} = Cracking strain of concrete
ε_{tu} = Ultimate tensile strain of concrete
ε_{sy} = Yield strain of reinforcement
ε_{su} = Ultimate strain of reinforcement
ν = Poisson's ratio
σ = Stress
σ_c = Compressive strength of the concrete
ρ_{min} = The minimum ratio of wall area to floor-plan area

REFERENCES

ASCE, 1982. Task committee on finite element analysis of reinforced concrete structures, State-of-the-art report on finite element analysis of reinforced concrete. ASCE, New York.

Ashour, A.F. and C.T. Morley, 1993. Three-dimensional nonlinear finite element modelling of reinforced concrete structures. Finite Elements Anal. Design, 15 (1): 43-55.

Bazant, Z.P. and B.H. Oh, 1983. Crack band theory for fracture of concrete. Mater. Struct., 16 (93): 155-177.

Bazant, Z.P., T. Belytschko, H. Yul-Woong and C. Ta-Peng, 1986. Strain-softening materials and finite-element solutions. Comput. Struct., 23 (2): 163-180.

Campione, G. and L. Mendola, 2004. Behavior in compression of reinforced concrete confined with transverse steel reinforcement. Cem. Concr. Composites, 26 (6): 645-656.

Chen, W.F., 1982. Plasticity in Reinforced Concrete. McGraw-Hill, New York.

Choi, C. and S. Cheung, 1996. Tension stiffening model for planar reinforced concrete members. Comput. Struct., 59 (1, 3): 179-190.

Chung, H., K. Yang, Y. Lee and H. Eun, 2002. Stress-strain curve of laterally confined concrete. Eng. Struct., 24 (9): 1153-1163.

Darwin, D. and D. Pecknold, 1977. Nonlinear biaxial stress-strain law for concrete. ASCE J. Eng. Mech. Division, 103 (EM4): 229-241.

Gupta, A.K. and S.R. Maestrini, 1989. Post-cracking behavior of membrane reinforced concrete elements including tension-stiffening. ASCE J. Struct. Eng., 115 (4): 957-993.

Gupta, A.K. and S.R. Maestrini, 1990. Tension-stiffness model for reinforced concrete bars. ASCE J. Struct. Eng., 116 (3): 769-790.

Hegemier, G.A., H. Murakami and L. Hageman, 1985. On tension stiffening in reinforced concrete. Mech. Mater., 4 (2): 161-179.

Kheyroddin, A., 1996. Nonlinear finite element analysis of flexure-dominant reinforced concrete structures. Ph.D Thesis, McGill University, Montreal, Canada, pp: 290.

Kheyroddin, A., M.A. Shayanfar and M.S. Mirza, 1997. Element size effects in nonlinear analysis of R.C. members. Comput. Struct., 62 (2): 339-352.

Kupfer, H.B., K.H. Gerstle and H. Rusch, 1969. Behavior of concrete under biaxial stresses. ACI Struct. J., 66 (8): 656-666.

Kwak, H. and D. Kim, 2004. Material nonlinear analyses of RC shear walls subject to cyclic loadings. Eng. Struct., 26 (10): 1423-1436.

Kwak, H. and D. Kim, 2006. Cracking behavior of RC panels subject to biaxial tensile stresses. Comput. Struct., 84 (5-6): 305-317.

Martín-Pérez, B. and S.J. Pantazopoulou, 2001. Effect of bond, aggregate interlock and dowel action on the shear strength degradation of reinforced concrete. Eng. Struct., 23 (2): 214-227.

Pastor, J.A., 1986. High-Strength Concrete Beams. Ph.D Thesis, Cornell University, New York, Ithaca.

Palermo, D. and F.J. Vecchio, 2004. Compression field modeling of reinforced concrete subjected to reversed loading: Verification. ACI Struct. J., 101 (2): 155-164.

Sundara, R.I.K.T., S. Raviraj and T.N. Jayaram, 2002. Analysis of crack propagation in strain-softening beams. Eng. Fracture Mech., 69 (6): 761-778.

van der Put, T.A.C.M., 2007. Softening behaviour and correction of the fracture energy. Theor. Applied Fracture Mech., 48 (2): 127-139.

Vecchio, F.J., 1999. Towards cyclic load modeling of reinforced concrete. ACI Struct. J., 96 (2): 389-407.

Vecchio, F.J. and D. Palermo, 2002. Behavior of three dimensional reinforced concrete shear walls. ACI Struct. J., 99 (1): 81-89.

Wallace, J.W. and J.H. Thomsen, 1995. Seismic design of RC structural walls. ASCE J. Struct. Eng., 121 (1): 88-101.

Zienkiewicz, O.C., R.L. Taylor and J.Z. Zhu, 2005. Inelastic and Non-Linear Materials. 6th Edn. The Finite Element Method Set.